PHYSICAL REVIEW D **88,** 114027 (2013)

Proton-air collisions in a model of soft interactions at high energies

E. Gotsman,[1] E. Levin,[1,2] and U. Maor[1]

[1]*Department of Particle Physics, School of Physics and Astronomy, Raymond and Beverly Sackler Faculty of Exact Science, Tel Aviv University, Tel Aviv 69978, Israel*

[2]*Departamento de Física, Universidad Técnica Federico Santa María, Avenida España 1680 and Centro Cientifico-Tecnolgico de Valparaíso, Casilla 110-V, Valparaíso, Chile*

(Received 2 September 2013; published 16 December 2013)

We evaluate both the Pomeron interactions and the inelastic Gribov corrections to the Glauber-Gribov formula, which is used to extract proton-proton cross sections from proton-air collisions at high energies. We demonstrate that these corrections are compatible with the errors for proton-air cross sections measured at ultrahigh energies in cosmic ray experiments. We present the results of a calculation of these cross sections based on our model for the soft interactions at high energies, which provides a good description of available accelerator data, including that for LHC energies.

DOI: 10.1103/PhysRevD.88.114027 PACS numbers: 13.85.−t, 13.85.Hd, 13.60.Hb, 11.55.−m

I. INTRODUCTION

The LHC data [1–4] provided two important lessons for our understanding of soft interactions at high energy. In the first, regrettably, none of the phenomenological models based on the Reggeon approach [5–8] were able to predict the data, in spite of having a number of fitting parameters. In the second, a more encouraging one, the LHC data could be fitted by choosing a new set of the parameters without changes in the theoretical scheme of the models. The natural question that arises is whether the new set of parameters has any predictable power, or whether its lifetime is only until new measurements at higher energies appear. In particular, we ask this question in relation to our model and to our final set of fitting parameters (see Ref. [9]). Our model has passed the first check: it is able to describe the proton-proton inelastic and total cross section at $W = 57$ TeV that has been extracted from the Pierre Auger Collaboration data on proton-air interactions [10]. These data are (in parentheses we put the prediction of our model [9])

$$\begin{aligned}\sigma_{pp}^{inel} &= [92 \pm 7(\text{stat})^{+9}_{-11}(\text{syst}) \pm 7(\text{Glauber})\,\text{mb}](95.2\,\text{mb})\\ \sigma_{pp}^{tot} &= [133 \pm 13(\text{stat})^{+17}_{-20}(\text{syst}) \pm 16(\text{Glauber})\,\text{mb}](130\,\text{mb})\end{aligned} \tag{1.1}$$

Our goal in this paper is to compare our model directly with the cosmic data on the proton-air interactions. We re-visit the problem of hadron-nucleus interactions at high energies. It is well known that the Glauber-Gribov approach[1] [11,12], where the total cross section of the hadron-nucleus interaction is expressed through the inelastic cross section of hadron-proton scattering, can only be justified at rather low energies, where corrections due to Pomeron interactions may be neglected. A more general approach has been developed [13–16] in which the Pomeron interactions have been taken into account in the energy range for

$$\begin{aligned}&gS_A(b)G_{3IP}e^{\Delta_{IP}Y} \propto gG_{3IP}A^{1/3}e^{\Delta_{IP}Y} \approx 1;\\ &gG_{3IP}e^{\Delta_{IP}Y} < 1; \qquad gG^2_{3IP}e^{\Delta_{IP}Y}e^{\Delta_{IP}Y} \ll 1,\end{aligned} \tag{1.2}$$

where G_{3IP} denotes the triple Pomeron coupling, g the vertex of Pomeron nucleon interaction, and $1 + \Delta_{IP}$ the Pomeron intercept. For the nuclear profile $S_A(b)$ we use the general expression

$$S_A(b) = \int_{-\infty}^{+\infty} dz\rho(z, b) \qquad \int d^2bS_A(b) = A, \tag{1.3}$$

where $\rho(z, b)$ is the density of nucleons in a nucleus.

In this approach, to calculate the hadron-nucleus cross sections, one needs to know the values of Δ_{IP}, g, and G_{3IP}.

In this paper we discuss the non-Glauber-type corrections to the hadron-nucleus interaction. Our reanalysis of the problem is based on two recent achievements.

First, the Auger Collaboration has published a measurement of the proton-air total cross section at extremely high energies ($W = 57$ TeV) with sufficiently small errors [$\sigma_{tot}(\text{p-Air}) = 505 \pm 22(\text{stat})^{+28}_{-36}(\text{syst})$ mb [10]].

Second, a model for high energy hadron-hadron scattering has been proposed that successfully describes the LHC data and that includes all the theoretical ingredients found in QCD and $N = 4$ supersymmetric Yang-Mills (SYM) [5,9]. The latter allows us to calculate the non-Glauber corrections and to estimate the influence of these corrections on the value of the proton-air cross section at very high energies.

In the next section we briefly review the main theoretical formulas for hadron-nucleus interactions. In Sec. III we

[1]We add to the Glauber approach the name of Gribov, in recognition of his interpretation of the Glauber formula in the parton approach and the creation of a space-time picture of the hadron-nucleus interaction, both of which are correct in QCD. The problem of Gribov's inelastic corrections will be discussed below.

 © 2013 American Physical Society

calculate the proton-air cross section using our model, all parameters of which have been determined by fits to the proton-proton data. In this section we estimate the difference between the Glauber-Gribov approach, and the alternative approach that includes the Pomeron interactions. In the conclusions we summarize our results.

II. HADRON-NUCLEUS COLLISIONS

A. Pomeron field theory: general approach, based on $N = 4$ SYM and QCD

Models describing soft interactions at high energy (see for example Refs. [5–8]) use Pomeron field theory (PFT) in slightly different forms. Our approach to PFT acquires a simple form when written in the framework of a functional integral:

$$Z[\Phi, \Phi^+] = \int D\Phi D\Phi^+ e^S \quad \text{with} \quad S = S_0 + S_I + S_E, \tag{2.1}$$

where

$$S_0 = \int dY \Phi^+(Y)\left\{-\frac{d}{dY} + \Delta_{IP}\right\}\Phi(Y) \tag{2.2}$$

describes the free Pomeron with an intercept Δ_{IP} and with $\alpha'_{IP} = 0$. Both in QCD [17] and in $N = 4$ SYM [18,19] we expect that Δ_{IP} should be rather large ($\Delta_{IP} = 0.2$–0.3) and $\alpha'_{IP} = 0$. These two features of the above theoretical approaches have been included in Eq. (2.2). S_I characterizes the interaction between Pomerons and takes the form

$$S_I = G_{3IP}\int dY\{\Phi(Y)\Phi^+(Y)\Phi^+(Y) + \text{H.c.}\}. \tag{2.3}$$

Note we only take into account the triple Pomeron interaction. Such a form provides a natural matching with the perturbative QCD approach [20] and the Balitsky-Fadin-Kuraev-Lipatov Pomeron calculus [21]. We will specify S_E, which is responsible for the interaction with the target and projectile considering two processes: proton-proton and proton-nucleus interactions. The PFT with the action given by Eqs. (2.2) and (2.3) has been solved (see Refs. [22,23]) for arbitrary S_E.

B. Proton-proton interaction

1. S_E for hadron-hadron collisions

We need to incorporate in our procedure a sufficiently large Good-Walker [24] component, which is required for describing diffraction in low masses, and which follows from the $N = 4$ SYM approach [19]. We develop a two channel model that takes into account the Good-Walker mechanism, and in which the observed physical hadronic and diffractive states are written in the form

$$\psi_h = \alpha\Psi_1 + \beta\Psi_2; \qquad \psi_D = -\beta\Psi_1 + \alpha\Psi_2, \tag{2.4}$$

where $\alpha^2 + \beta^2 = 1$. Note that Good-Walker diffraction is presented by a single wave function ψ_D. Wave functions Ψ_1 and Ψ_2 diagonalize the interaction matrix, which has the form

$$A^{i',k'}_{i,k} = \langle\Psi_i\Psi_k|\mathbf{T}|\Psi_{i'}\Psi_{k'}\rangle = A_{i,k}\delta_{i,i'}\delta_{k,k'}. \tag{2.5}$$

The unitarity constraints can be written

$$\text{Im}A_{i,k}(s, b) = |A_{i,k}(s, b)|^2 + G^{\text{in}}_{i,k}(s, b), \tag{2.6}$$

where $G^{\text{in}}_{i,k}(s, b)$ is the probability for all inelastic processes induced by the initial (i, k) states.

Bearing in mind Eq. (2.4) we can write S_E in the form

$$S_E = -\int dY' d^2b \sum_{i=1}^{2}\{\Phi(Y')g^{(i)}(b)\delta(Y' - 0) + \Phi(Y')g^{(i)}(b)\delta(Y - Y')\}, \tag{2.7}$$

where $g^{(i)}$ denotes the vertex of the Pomeron interaction with the state i, which is described by the wave function either Ψ_1 or Ψ_2. $Y' = 0$ ($Y' = Y$) indicate, respectively, the position of the target and projectile in rapidity, and b the impact parameter. We parametrize $g^{(i)}(b)$ as

$$g^{(i)}(b) = g^{(i)}S(b) = \frac{g^{(i)}}{4\pi}m_i^3 bK_1(m_i b), \tag{2.8}$$

where $S(b)$ is the Fourier transform of the dipole formula for the form factor $1/(1 + q^2/m_i^2)^2$. $K_1(z)$ is the modified Bessel function of the second kind, the McDonald function [see Ref. [25] formula (8.4)].

2. Small parameters and selection of the Pomeron diagrams

Using Eqs. (2.1), (2.2), (2.3), and (2.7) we can find expressions for all experimental observables for the proton-proton interaction.[2] However, we simplify the problem by defining a new small parameter, viz.,

$$Q = \gamma^2 s^{\Delta_{IP}} \ll 1, \quad \text{while } H = g^{(i)}G_{3IP}s^{\Delta_{IP}} \geq 1 \tag{2.9}$$

in the process of fitting the experimental data. In Table I we display the values of the parameters in our model and check that Eq. (2.9) is satisfied for any reasonable energy. In Eq. (2.9) $\gamma^2 = \int G^2_{3IP}(k_{T,1} = 0, k_T, k_T)d^2k_T$, where $k_{T,i}$ are transverse momenta of three Pomerons. The main contributions, which are proportional to H^n, stem from the "net" diagrams of Fig. 1(a). The small parameter Q comes from the diagram of Fig. 1(b) and describes the interaction between two Pomerons that are not attached to the proton or the Pomeron loop diagrams [see two examples in Fig. 1(b)].

[2]We need to introduce additional phenomenological parameters to describe the main characteristics of the inelastic processes, which take into account the hadronization stage, in terms of the microscopic approach based on QCD.

TABLE I. Fitted parameters for our model. The quality of the fit is $\chi^2/\text{d.o.f.} = 0.86$.

Δ_{IP}	β	α'_{IP} (GeV^{-2})	g_1 (GeV^{-1})	g_2 (GeV^{-1})	m_1 (GeV)	m_2(GeV)	γ	G_{3IP} (GeV^{-1})	$\tilde{g}$ (GeV^{-1})
0.23	0.46	0.028	1.89	61.99	5.045	1.71	0.0045	0.03	14.6

In our model we sum all diagrams proportional to H^n, where n is the number of the triple Pomeron vertices. We do this summation using the Mueller-Patel-Salam-Iancu (MPSI) approximation [26], which was adapted to our problem in Ref. [5]. We do not discuss this approximation here; Fig. 2 illustrates its main features. It shows a typical net diagram. Integration over rapidities Y' and Y'' leads to many contributions of this diagram, and in the MPSI approximation we only consider that contribution that is proportional to $e^{3\Delta_{IP}Y}$, neglecting all other terms that have at least one factor $e^{\Delta_{IP}Y}$ less. Since Δ_{IP} is large in our model, the MPSI approximation provides sufficient accuracy for our calculations.

3. Scattering amplitudes and experimental observables

In the model we introduce the amplitudes

$$A_{i,k}(s,b) = i\left(1 - \exp\left(-\frac{\Omega_{i,k}(s,b)}{2}\right)\right),$$
$$G^{\text{in}}_{i,k} = 1 - \exp\left(-\Omega_{i,k}(s,b)\right), \tag{2.10}$$

which satisfy the unitarity constraints of Eq. (2.6). Summing the net diagrams we obtain

$$\Omega_{i,k}(Y;b) = \int d^2b' \frac{g^{(i)}(\vec{b}')g^{(k)}(\vec{b}-\vec{b}')e^{\Delta_{IP}Y}}{1 + G_{3IP}e^{\Delta_{IP}Y}[g^{(i)}(\vec{b}') + g^{(k)}(\vec{b}-\vec{b}')]}. \tag{2.11}$$

We include the summation of the enhanced diagrams (see Fig. 3) in addition to the net diagrams. These diagrams sum contributions proportional to the small parameter Q^n and change the intercept of the soft Pomeron. We use them to control the accuracy of our calculations.

The summation of the enhanced diagrams in the MPSI approximation results in a new Pomeron propagator that replaces $e^{\Delta_{IP}Y}$ in Eq. (2.11).

$$e^{\Delta_{IP}Y} \to G_{\text{enh}}(Y) = \frac{1}{\gamma}\left(1 - \exp\left(\frac{1}{T(Y)}\right)\frac{1}{T(Y)}\Gamma\left(0, \frac{1}{T(Y)}\right)\right). \tag{2.12}$$

$\Gamma(0,x)$ is the incomplete Gamma function [see (8.350)–(8.359) in Ref. [25]], and $T(Y)$ is given by

$$T(Y) = \gamma e^{\Delta_{IP}Y}. \tag{2.13}$$

Finally, the amplitudes for proton-proton scattering can be calculated in terms of the amplitude $A_{ik}(b)$ as follows:

$$\text{elastic amplitude: } a_{\text{el}}(b) = (\alpha^4 A_{1,1} + 2\alpha^2\beta^2 A_{1,2} + \beta^4 A_{2,2}); \tag{2.14}$$

$$\text{G-W single diffraction: } a^2_{\text{sd}}(b) = 2|\alpha\beta\{-\alpha^2 A_{1,1} + (\alpha^2 - \beta^2)A_{1,2} + \beta^2 A_{2,2}\}|^2; \tag{2.15}$$

$$\text{G-W double diffraction: } a^2_{\text{dd}}(b) = \alpha^4\beta^4|A_{1,1} - 2A_{1,2} + A_{2,2}|^2. \tag{2.16}$$

4. Description of the experimental data

At the end of this section we will discuss the experimental data that we are able to describe using our model. First, we obtain a good fit of all soft cross section data: σ_{tot}, σ_{el}, σ_{sd}, and σ_{dd} in the wide range of energy from $W = 20$ GeV to 7 TeV [9]. We are also

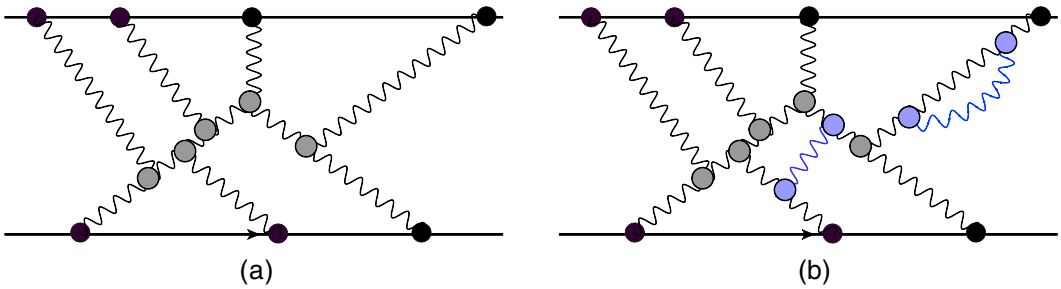

FIG. 1 (color online). The set of diagrams that contribute to the scattering amplitude of proton-proton scattering in the kinematic region given by Eq. (2.9). (a) The net diagrams that are proportional to H^n. (b) Two examples of the diagrams that are proportional to an additional power of the small parameter Q. The figure that is proportional to an extra Q^2 was neglected. The wavy lines denote the soft Pomerons. The black circles denote $g^{(i)}$, while the gray circles describe the triple Pomeron vertices.

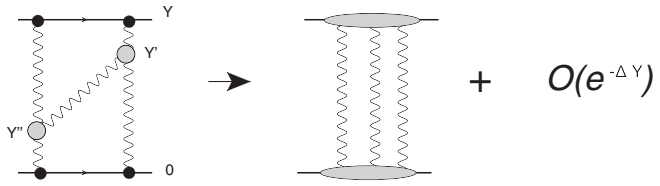

FIG. 2. The first net diagram in the MPSI approximation for proton-proton scattering.

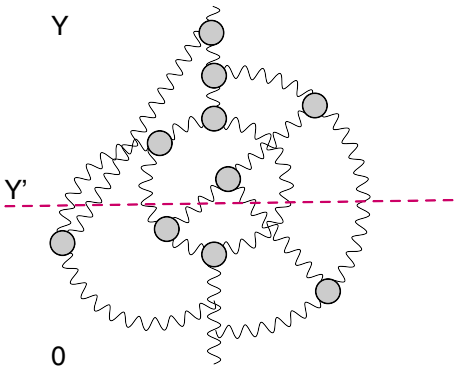

FIG. 3 (color online). The set of enhanced diagrams for the soft Pomeron.

able to reproduce $d\sigma_{\rm el}/dt$ for $t < 0.5$ GeV^2, as well as the elastic slope [9]. We found that our model reproduces experimental behavior of $dN/d\eta$ [27]. In our recent paper we describe the multiplicity distribution at $W = 7$ TeV [28]. Hence, we conclude that our model successfully describes all available accelerator data. To satisfy the request of our referee, we have included Fig. 4, which appeared in our paper [9], and which displays a comparison of our predictions and the corresponding experimental data.

C. Hadron-nucleus interaction

1. S_E for hadron-nucleus scattering

Using Eq. (2.7) and neglecting the correlations between nucleons in a nucleus, the S_E term can be written in the form

$$S_E = -\int dY' d^2b \sum_{i=1}^{2} \{\Phi(Y') g^{(i)}(b)\delta(Y - Y') + \Phi(Y') \times \int d^2b' g^{(i)}(\vec{b} - \vec{b}') S_A(b')\delta(Y' - 0)\}. \quad (2.17)$$

The last term is well known, and we refer the reader to Refs. [21,29], which, as far as we know, are the most recent papers where this derivation has been based on Feynman diagrams. For heavy nuclei $|\vec{b} - \vec{b}'| \ll R_A$ and the second term in Eq. (2.17) can be replaced by

$$\Phi(Y') \int d^2b' g(i)(\vec{b} - \vec{b}') S_A(b') \overset{|\vec{b}-\vec{b}'| \ll R_A}{\longrightarrow} \Phi(Y') g^{(i)} S_A(b). \quad (2.18)$$

However, in the case of air, the radii of nitrogen and oxygen are not very large, and we cannot neglect the b' dependence.[3]

2. Glauber-Gribov formula

When discussing the hadron-nucleus interaction we always start with the Glauber-Gribov formula, which sums the diagrams of Fig. 5 and takes the following form:

$$\sigma^{\rm hA}_{\rm in} = \int d^2b \Big(1 - \exp\Big(-\int d^2b' \{2\,{\rm Im} a_{\rm el}(s, \vec{b} - \vec{b}') - |a_{\rm el}(s, \vec{b} - \vec{b}')|^2\} S_A(b')\Big)\Big). \quad (2.19)$$

This formula can be proven just by direct summation of the diagrams in Fig. 5(a). In the case when the wave function of the proton diagonalizes the interaction matrix [$\alpha = 1$, $\beta = 0$ in Eq. (2.4)] the term in $\{\cdots\}$ of Eq. (2.19) gives $G^{\rm in}(s, b)$ for the hadron-proton interaction. In the case of Eq. (2.18) the Glauber-Gribov formula takes the familiar form

$$\sigma^{\rm hA}_{\rm in} = \int d^2b (1 - \exp(-\sigma^{\rm in}_{pp} S_A(b))). \quad (2.20)$$

3. Gribov's inelastic corrections

Gribov's inelastic corrections [12] to Eq. (2.19) stem from processes of diffraction dissociation in hadron-proton scattering. In our approach we introduce a two channel model to describe the Good-Walker mechanism of the low mass diffraction. In the framework of this mechanism, taking into account Gribov's inelastic corrections, reduces to the summation of the same diagrams as in Fig. 5, and has been considered in Sec. II C 1, here the interaction with the nucleons in the nucleus has a more complicated form. The result is

$$\sigma^{\rm hA}_{\rm in} = \int d^2b \Big(1 - \exp\Big(-\int d^2b' \{2\,{\rm Im} a_{\rm el}(s, \vec{b} - \vec{b}') - |a_{\rm el}(s, \vec{b} - \vec{b}')|^2 - a^2_{\rm sd}(s, \vec{b} - \vec{b}') - a^2_{\rm dd}(s, \vec{b} - \vec{b}')\} S_A(b')\Big)\Big). \quad (2.21)$$

Substituting Eqs. (2.14), (2.15), and (2.16) into this equation we obtain, using the unitarity constraints of Eq. (2.6), that

$$\{\cdots\} = \alpha^4 G^{\rm in}_{1,1} + 2\alpha^2\beta^2 G^{\rm in}_{1,2} + \beta^4 G^{\rm in}_{2,2}, \quad (2.22)$$

[3]We thank our referee, who pointed out that this correction could be rather large, especially at high energies, due to the shrinkage of the diffraction peak.

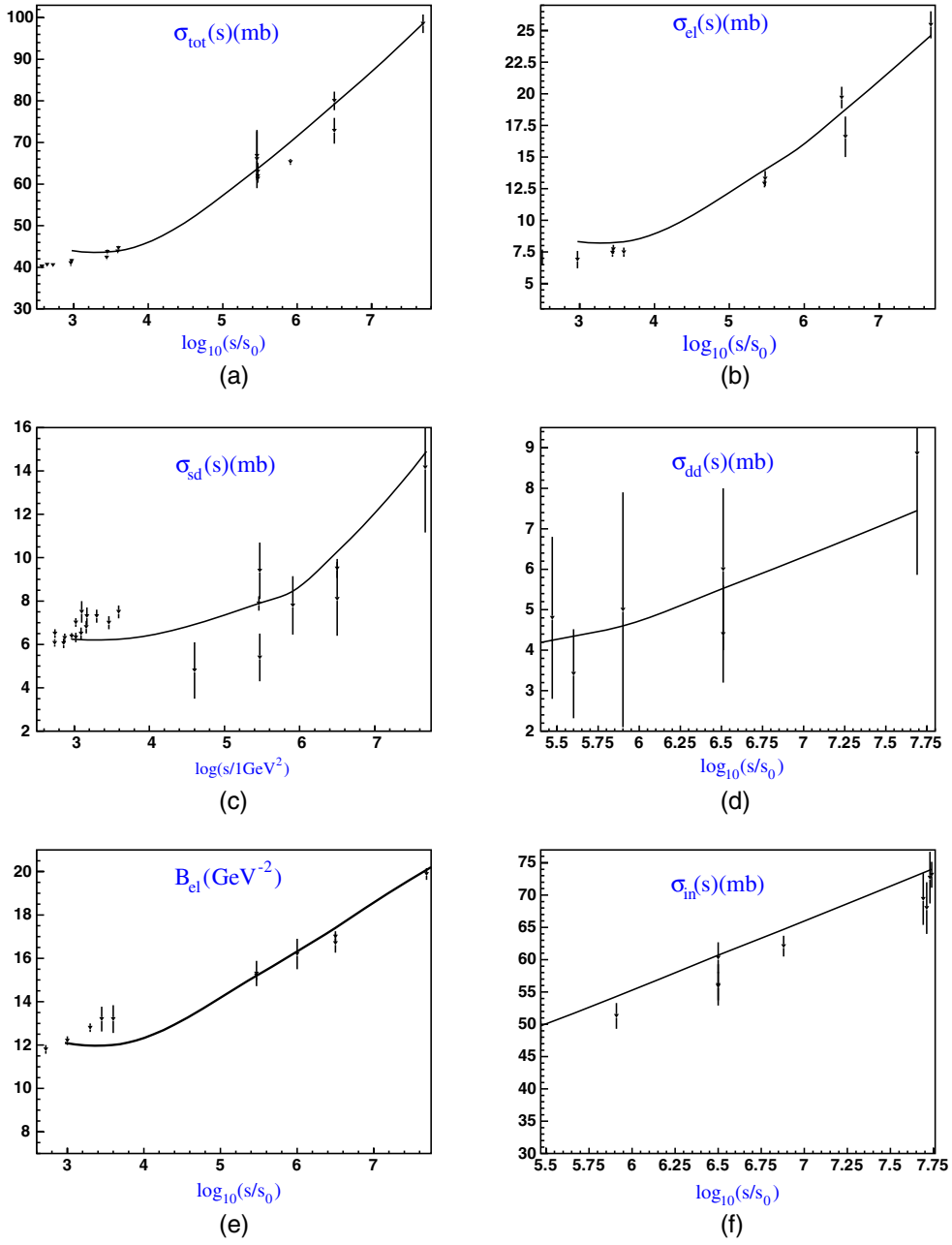

FIG. 4 (color online). The energy behavior of the total (a), elastic (b), single diffraction (c), double diffraction (d), and inelastic (f) cross sections and elastic slope (e), compared with experimental data. The solid lines show the results of our present fit. The data have been taken from Ref. [36] for energies less than the LHC energy. At the LHC energy for total and elastic cross sections we use TOTEM data [4], and for single and double diffraction cross sections are taken from Ref. [1].

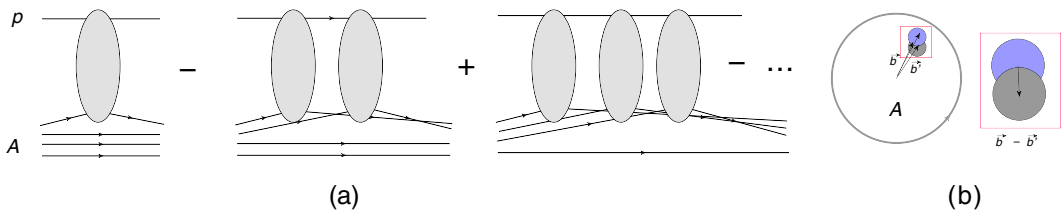

FIG. 5 (color online). The Glauber-Gribov formula for the hadron-nucleus interaction. (a) Blobs denote nucleon-nucleon interactions, while solid lines correspond to nucleons in the nucleus. (b) The open circles represent the nucleus while the filled circles denote the nucleons.

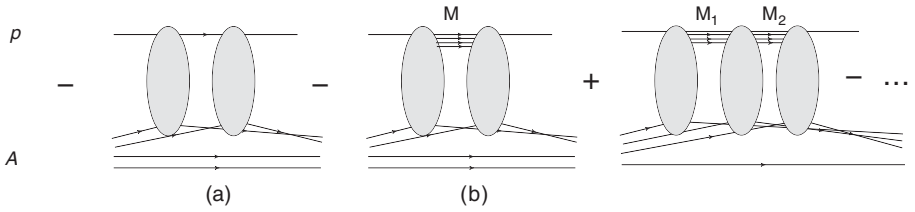

FIG. 6. The inelastic corrections to the Glauber-Gribov formula for the hadron-nucleus interaction. Blobs denote nucleon-nucleon interactions, while solid lines represent nucleons.

which is the amplitude of the inelastic interaction for the incoming proton [see Eq. (2.14) for comparison]. Using Eqs. (2.18) and (2.21) reduces to the Glauber-Gribov formula with one difference: instead of $\sigma_{\rm in} = \sigma_{\rm tot} - \sigma_{\rm el}$ in the formula we have $\sigma_{\rm in} = \sigma_{\rm tot} - \sigma_{\rm el} - \sigma_{\rm dif}$, where $\sigma_{\rm dif} = 2\sigma^{\rm GW}_{\rm sd} + \sigma^{\rm GW}_{\rm dd}$, as was advocated in Ref. [30,31]. Note, that the low mass of both single and double diffractions enters Eq. (2.21).

We wish to emphasize that Eq. (2.21) sums all diagrams, given by Fig. 5, which are related to Gribov's inelastic corrections. However, there exist other corrections that are shown in Fig. 6. In the next section we sum these corrections for the large produced masses (M, M_1, and M_2 in Fig. 6), and this summation leads to Eq. (2.24). We have neglected the contributions with small masses that correspond to the Good-Walker mechanism. The reasons for this are the following. First, the contamination of the proton wave function by the diffractive state is small in our model ($\beta^2 = 0.21$). Second, we have natural small parameters, $\frac{1}{2}\sigma_{\rm sd}/\sigma_{\rm el}$ and $\sigma_{\rm dd}/\sigma_{\rm el}$, where $\sigma_{\rm sd}$, $\sigma_{\rm dd}$, and $\sigma_{\rm dd}$ denote the single, double diffractive, and elastic cross sections for proton-proton collisions. For $W = 57$ TeV the ratios are equal to 0.17 and 0.23, respectively. We note that the ratio of the contributions of the diagram Fig. 6(b) to the diagram Fig. 6(a) is equal to $\frac{1}{2}\sigma_{\rm sd}/\sigma_{\rm el}$. Third, the difference between Eqs. (2.19) and (2.21) turns out to be rather small (see Figs. 10 and 11 below) for the inelastic hadron-nucleus collisions. However, for the total cross sections the difference is more pronounced and the neglected corrections could be important. The method for calculating them is known (see Ref. [31]), and we intend to reevaluate our estimates for the total cross sections when the data at high energies become available.

At this point of our presentation, we wish to emphasize that the goal of this paper is neither to discuss the most general formula for hadron-nucleus collision in the framework of the Pomeron calculus nor to estimate the corrections to the Pomeron calculus, but to check whether our set of the phenomenological parameters can provide a reasonable description of the experimental data at ultrahigh energies.

4. Inelastic corrections due to Pomeron interaction

The Glauber-Gribov formula, even with Gribov's inelastic corrections, describes the hadron-nucleus interactions only, if we neglect the triple Pomeron interaction, i.e., considering S_I of Eq. (2.3) equal to zero. In general, we cannot solve the problem, but in the kinematic region of Eq. (1.2), the hadron-nucleus scattering amplitude can be written in an eikonal form in which the opacity Ω is given by sum of the "fan" diagrams [13,15,16,32] [see Fig. 7(b)].

The scattering amplitude can be written in the form

$$A_{\rm hA}(Y, b) = i\left(1 - \exp\left(-\frac{\Omega_{\rm hA}(Y; b)}{2}\right)\right), \tag{2.23}$$

where Ω sums all $h - A$ irreducible diagrams.

In the region of Eq. (1.2) all diagrams proportional to $(gS_A(b)G_{3IP}e^{\Delta_{IP}Y})^n$, where n is the number of the triple Pomeron vertices, are shown in Fig. 7(b). Their sum takes the form (see Ref. [16] for details)

$$\Omega_{\rm hA}(Y; b) = \int d^2b' d^2b'' \frac{g_h(b')\tilde{g}(b'')G_{\rm enh}(Y)S_A(\vec{b} - \vec{b}' - \vec{b}'')}{1 + \int d^2\hat{b}\,\tilde{g}(\hat{\vec{b}})G_{3IP}G_{\rm enh}(Y)S_A(\vec{b} - \vec{b}' - \hat{\vec{b}})}, \tag{2.24}$$

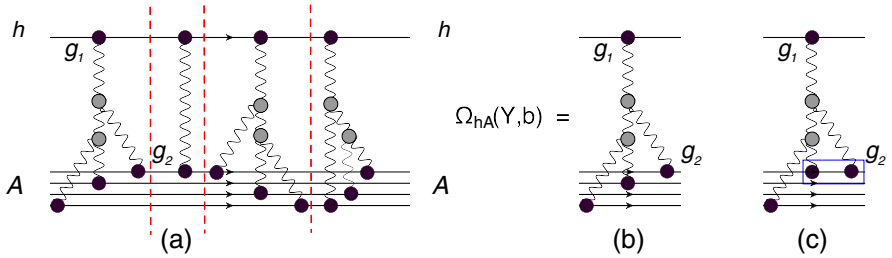

FIG. 7 (color online). The set of diagrams that contributes to the scattering amplitude of hadron-nucleus scattering in the kinematic region given by Eq. (1.2). (b) The hadron-nucleus irreducible diagrams while the general case is shown in (a). (c) The correction to the value of Ω. The vertical dashed lines indicate the hadron-nucleus states. The wavy lines denote the soft Pomerons.

where $\tilde{g}(b) = \alpha^2 g^{(1)}(b) + \beta^2 g^{(2)}(b)$. The integral $\tilde{g} = \int d^2b \tilde{g}(b)$ is shown in Table I.

For diagrams of Fig. 7, $G_{\rm enh}(Y)$ is the Green's function of the Pomeron exchange, which is equal to

$$G_{\rm enh}(Y) = e^{\Delta_{IP} Y}. \tag{2.25}$$

In Fig. 7(c) the correction to the main contribution is plotted, in which one of $(gS_A(b)G_{3IP}e^{\Delta_{IP}Y})$ is replaced by $(gG_{3IP}e^{\Delta_{IP}Y})$. Using the MPSI approximation that has been adapted to our model in Ref. [5], we calculate Ω_1 [Fig. 7(c)] and Ω_2 [Fig. 7(b)]. We obtain

$$\frac{\Omega_1}{\Omega_2} = \frac{gG_{3IP}G_{\rm enh}(Y)}{(1 + gG_{3IP}G_{\rm enh}(Y)S_A())^2 b} \ll 1. \tag{2.26}$$

Indeed, at low energy where $gG_{3IP}G_{\rm enh}(Y)S_A(\vec{b}) < 1$ this ratio is of the order of $1/S_A(b) < 1$. For high energy it decreases as $e^{-\Delta_{IP}Y}$.

A word of caution should be added here, since Eq. (2.26) is derived in the kinematic region of Eq. (1.2), this equation does not describe the contribution at very large impact parameters $b \gg R_A$ where $S_A(b) \ll 1$ and Eq. (1.2) cannot be applied here. However, we believe that this region is not responsible for the main contribution for the inelastic hadron-nucleus collision.

From Eqs. (2.23) and (2.24), we have

$$\begin{aligned}
\sigma^{\rm hA}_{\rm tot} &= 2\int d^2b\left(1 - \exp\left(-\frac{\Omega_{\rm hA}(Y;b)}{2}\right)\right);\\
\sigma^{\rm hA}_{\rm el} &= \int d^2b\left(1 - \exp\left(-\frac{\Omega_{\rm hA}(Y;b)}{2}\right)\right)^2;\\
\sigma^{\rm hA}_{\rm in} &= \int d^2b(1 - \exp\left(-\Omega_{\rm hA}(Y;b)\right)).
\end{aligned} \tag{2.27}$$

The processes of diffractive production have been discussed in Refs. [15,32].

5. Pomeron interaction and realistic proton-proton interaction

In Sec. C-4 we took into account the Pomeron interaction in the kinematic region of Eq. (1.2). In this section we develop an approximation in which we treat the proton-proton scattering using different small parameters, as has been discussed in Sec. II. The general equation for the opacity $\Omega_{\rm hA}(Y;b)$ is displayed in Fig. 8, and the blob denotes the proton-proton amplitude in our approach: Good-Walker mechanism + net Pomeron diagrams. The interaction with the nucleons of the nuclei is still determined by large parameters of Eq. (1.2) and has a simple form of the fan diagrams. Because of the simple form of our action [see Eqs. (2.1), (2.2), (2.3), and (2.17)] we can sum all diagrams in Fig. 8. Indeed, due to the fact that $\alpha'_{IP} = 0$ and G_{3IP} does not depend on the impact parameter, the interaction shown in Fig. 8 does not interfere with the structure of the diagram for proton-proton scattering and can be written in a factorizable form. A simple calculation in this spirit has been discussed in Ref. [16] and leads to the following expression for the opacity $\Omega_{\rm hA}(Y;b)$:

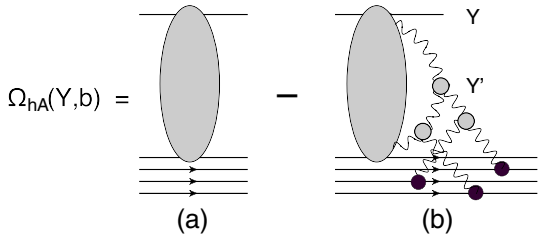

FIG. 8 (color online). The set of diagrams for Ω with realistic proton-proton interaction, including the Pomeron interactions in the kinematic region given by Eq. (1.2). Wavy lines denote the soft Pomerons, and black circles correspond to Pomeron-nucleon vertices. Blobs denote nucleon-nucleon interactions, solid lines correspond to nucleons. Grey circles denote triple Pomeron couplings.

$$\Omega_{\rm hA}(Y;b) = \int d^2b' A_{\rm pp}(Y, \vec{b} - \vec{b}')\mathcal{S}_A(Y;\vec{b}'); \tag{2.28}$$

$$\mathcal{S}_A(Y;\vec{b}') = \frac{S_A(\vec{b}')}{1 + \int d^2\hat{b}\, \tilde{g}(\hat{\vec{b}})G_{3IP}G_{\rm enh}(Y)S_A(\vec{b}' - \hat{\vec{b}})}. \tag{2.29}$$

The final formula that includes both the Good-Walker mechanism of low mass diffraction production and the enhanced Pomeron diagrams is

$$\begin{aligned}
&\sigma_{\rm in}(p + A;Y) = \int d^2b\left(1 - \exp\left(-\left\{2\,{\rm Im}a^{\rm el}_{\rm pp}(Y, \vec{b} - \vec{b}')\mathcal{S}_A(Y;\vec{b}') - [\sigma_{\rm el}(Y, \vec{b} - \vec{b}') + \sigma_{\rm diff}(Y, \vec{b} - \vec{b}')]\frac{\mathcal{S}^2_A(Y;\vec{b}')}{S_A(\vec{b}')}\right\}\right)\right);\\
&\sigma_{\rm el}(Y, \vec{b} - \vec{b}') + \sigma_{\rm diff}(Y, \vec{b} - \vec{b}') = |a^{\rm el}_{\rm pp}(Y, \vec{b} - \vec{b}')|^2 + |a^{\rm sd}_{\rm pp}(Y, \vec{b} - \vec{b}')|^2 + |a^{\rm dd}_{\rm pp}(Y, \vec{b} - \vec{b}')|^2.
\end{aligned} \tag{2.30}$$

6. A simple model

We consider the simplest model for proton-proton interaction, in which elastic and diffraction processes are taken into account (see Fig. 9), and which illustrates the main ingredients of our approach. In this model the main contribution stems from single Pomeron exchange. The contribution to $\sigma_{\rm in} = 2\sigma_{\rm tot} - \sigma_{\rm el} - \sigma_{\rm diff}$ is shown in Fig. 9(a). The Pomeron interaction [see Fig. 9(c)] is given by Eq. (2.30).

III. COMPARISON WITH THE EXPERIMENT

Before comparing with the experimental results, we would like to draw the reader's attention to the fact that

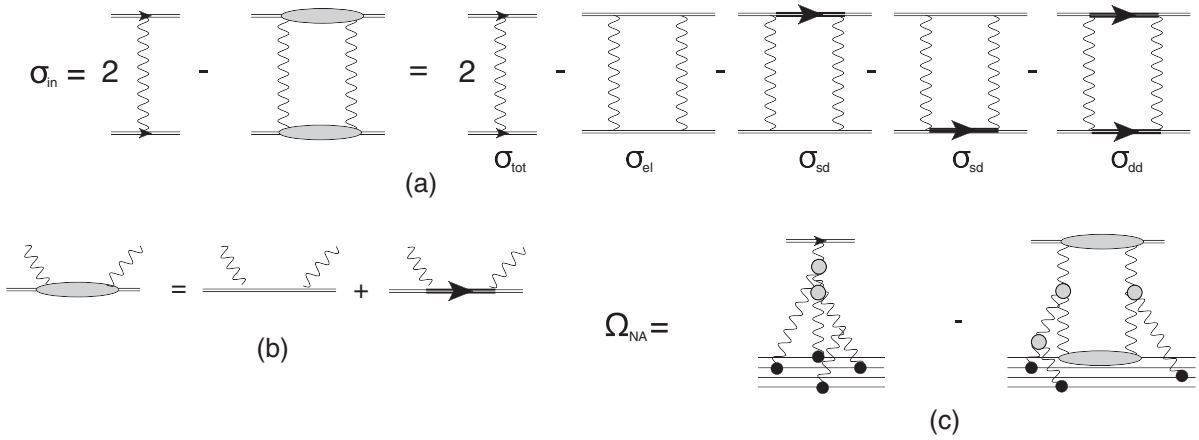

FIG. 9. Proton-nucleus interaction (c) in the simple model of (a) and (b). The thick arrows denote the exited states.

some of the experimental results shown might be overestimated, due to the possibility of the air showers being created by helium nuclei, as well as protons. The importance of this phenomena has been investigated by Block [33] and the Pierre Auger Collaboration [10]. We refer the reader to these references for further details. In the paper of the Pierre Auger Collaboration, a possible contamination of 25% of helium was assumed, which produces an uncertainty of about 30 mb (which is less than 10% of their final result), and is included in their systematic error.

The results of our calculations are shown in Fig. 10. For our calculations we used the parameters of our model, presented in Table I. For the scattering with air we use $S_{\rm Air}(b) = 0.78S_{\rm Ng}(b) + 0.22S_{\rm O}(b)$ where Ng and O denote nitrogen and oxygen, respectively. For both these nuclei we used the harmonic oscillator parametrization, following Ref. [34].

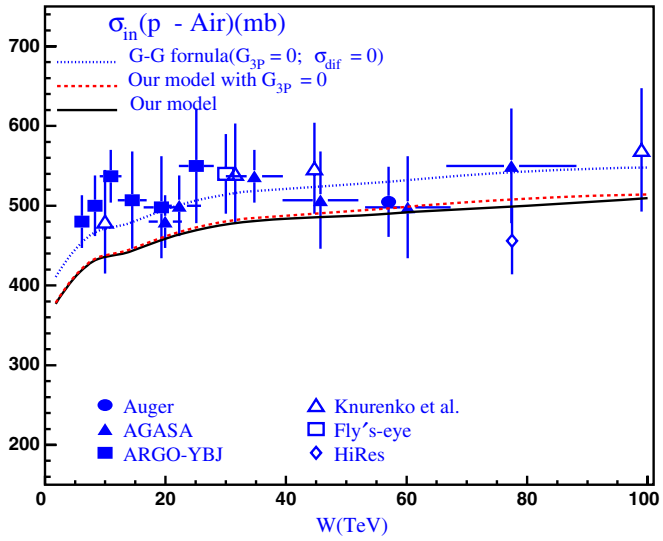

FIG. 10 (color online). Comparison of the calculated energy dependence of the total cross section for proton-air interactions with the high energy experimental data. Data are taken from Refs. [37–41]. $p_{\rm lab} = W^2/(2m)$ where m denotes the proton mass.

Two conclusions follow from the results of our calculations. First, all formulas, including the Glauber-Gribov one, give good agreement with the experimental data. This agreement improves (at least does not deteriorate) at ultra-high energies beyond the accelerator region ($W > 8$ TeV).

Second, the inelastic Gribov corrections (in Fig. 10 the curve with $G_{3IP} = 0$) decrease the value of the inelastic p-air cross section by 7%–10%, which are within the experimental errors. The corrections due to the Pomeron interaction turn out to be negligibly small (see our model curve in Fig. 10). We would like to stress that our model [5] gives a smaller contribution for Pomeron interactions when compared to other attempts to describe the LHC data [7,8].

We also calculate the total and inelastic cross sections for proton-lead interaction at high energy, to check whether the corrections due to Pomeron interactions are visible in the collisions with heavy nuclei. For a heavy nucleus such as lead we can use Eq. (2.18), and our prediction will not depend on the details of b distribution for the

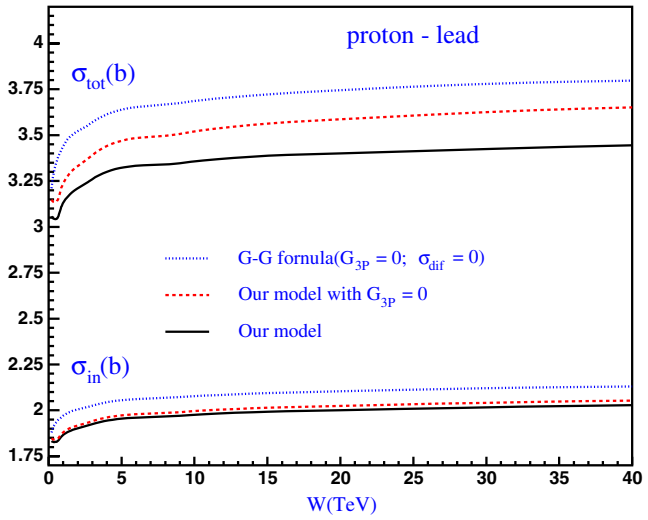

FIG. 11 (color online). Our model predictions for proton-lead cross sections. In this figure σ is in barns while W is in TeV.

proton-proton scattering. We employ the Wood-Saxon parametrization for $S_A(b)$

$$S_A(b) = \int_{-\infty}^{\infty} dz \frac{\rho_0}{1 + \exp\left(\frac{\sqrt{z^2+b^2}-R_A}{h}\right)}. \quad (3.1)$$

Figure 11 shows our predictions for the total and inelastic cross sections for the proton-lead interaction at high energy. For heavy nuclei the difference between our approach and the Glauber-Gribov formula is not large, reaching about 11% for the total and 5% for the inelastic cross sections. It is instructive to note that the inelastic cross section for heavy nuclei is not sensitive to Pomeron interactions, and the major difference from the Glauber-Gribov formula stems from the Good-Walker mechanism for low mass diffraction in proton-proton collisions. However, all three contributions influence the value and energy behavior of the total cross sections.

IV. CONCLUSIONS

In this paper we show that the set of parameters (see Table I) that describes the proton-proton interaction for the energy range $W = 20$ GeV–8 TeV provides a good description of the values and energy dependence of p-air cross sections at ultrahigh energies ($W > 1$ TeV). This supports our hypothesis that this set of parameters can be useful for predicting soft observables at high energies.

We found that both Gribov's inelastic corrections and Pomeron interactions lead to contributions that are in the range of present experimental errors. Our estimates show that the measurement of the total cross section for the interaction of a proton with heavy nuclei can be useful in the extraction of the different contributions of the non-Glauber type.

In the paper we did not discuss the correlation between nucleons in the nucleus, which we neglected in the Glauber-Gribov approach [35]. These correlations can give a considerable contribution, but they are beyond the scope of this paper.

ACKNOWLEDGMENTS

This research was supported by the Fondecyt (Chile) Grant No. 1100648.

[1] M. G. Poghosyan, J. Phys. G **38**, 124044 (2011); K. Aamodt *et al.* (ALICE Collaboration), Eur. Phys. J. C **65**, 111 (2010).
[2] G. Aad *et al.* (ATLAS Collaboration), Nat. Commun. **2**, 463 (2011).
[3] CMS Physics Analysis Summary, "Measurement of the inelastic pp cross section at s = 7 TeV with the CMS detector," 2011.
[4] F. Ferro (TOTEM Collaboration), AIP Conf. Proc. **1350**, 172 (2011); G. Antchev *et al.* (TOTEM Collaboration), Europhys. Lett. **96**, 21002 (2011); G. Antchev *et al.* (TOTEM Collaboration), Europhys. Lett. **95**, 41001 (2011).
[5] E. Gotsman, E. Levin, and U. Maor, Eur. Phys. J. C **71**, 1553 (2011); E. Gotsman, E. Levin, U. Maor, and J. S. Miller, Eur. Phys. J. C **57**, 689 (2008).
[6] A. B. Kaidalov and M. G. Poghosyan, arXiv:0909.5156.
[7] A. D. Martin, M. G. Ryskin, and V. A. Khoze, arXiv:1110.1973.
[8] S. Ostapchenko, Phys. Rev. D **83**, 014018 (2011).
[9] E. Gotsman, E. Levin, and U. Maor, Phys. Lett. B **716**, 425 (2012); Phys. Rev. D **85**, 094007 (2012).
[10] P. Abreu *et al.* (Pierre Auger Collaboration), Phys. Rev. Lett. **109**, 062002 (2012).
[11] R. J. Glauber, *Lectures in Theoretical Physics*, edited by W. E. Britten *et al.* (Interscience, New York, 1959) Vol. 1, p. 315.
[12] V. N. Gribov, Zh. Eksp. Teor. Fiz. **56**, 892 (1969) [Sov. Phys. JETP **29**, 483 (1969)]; Zh. Eksp. Teor. Fiz. **57**, 1306 (1969) [Sov. Phys. JETP **30**, 709 (1970)].
[13] A. Schwimmer, Nucl. Phys. **B94**, 445 (1975).
[14] A. Kaidalov, Nucl. Phys. **A525**, 39 (1991).
[15] S. Bondarenko, E. Gotsman, E. Levin, and U. Maor, Nucl. Phys. **A683**, 649 (2001).
[16] E. Gotsman, A. Kormilitzin, E. Levin, and U. Maor, Nucl. Phys. **A842**, 82 (2010), and references therein.
[17] E. A. Kuraev, L. N. Lipatov, and F. S. Fadin, Sov. Phys. JETP **45**, 199 (1977); I. I. Balitsky and L. N. Lipatov, Sov. J. Nucl. Phys. **28**, 822 (1978).
[18] A. V. Kotikov, L. N. Lipatov, A. I. Onishchenko, and V. N. Velizhanin, Phys. Lett. B **595**, 521 (2004); **632**, 754(E) (2006); A. V. Kotikov and L. N. Lipatov, Nucl. Phys. **B582**, 19 (2000); A. V. Kotikov, L. N. Lipatov, and V. N. Velizhanin, Phys. Lett. B **557**, 114 (2003).
[19] R. C. Brower, J. Polchinski, M. J. Strassler, and C. I. Tan, J. High Energy Phys. 12 (2007) 005; R. C. Brower, M. J. Strassler, and C. I. Tan, J. High Energy Phys. 03 (2009) 092; 03 (2009) 050.
[20] J. Bartels and M. Wusthoff, Z. Phys. C **66**, 157 (1995).
[21] M. A. Braun, Phys. Lett. B **483**, 115 (2000); Eur. Phys. J. C **33**, 113 (2004); Phys. Lett. B **632**, 297 (2006); Eur. Phys. J. C **48**, 511 (2006); Phys. Lett. B **483**, 115 (2000).
[22] D. Amati, M. Le Bellac, G. Marchesini, and M. Ciafaloni, Nucl. Phys. **B112**, 107 (1976); D. Amati, G. Marchesini, M. Ciafaloni, and G. Parisi, Nucl. Phys. **B114**, 483 (1976).
[23] M. Kozlov and E. Levin, Nucl. Phys. **A779**, 142 (2006).
[24] M. L. Good and W. D. Walker, Phys. Rev. **120**, 1857 (1960).
[25] I. Gradstein and I. Ryzhik, *Tables of Series, Products, and Integrals* (Verlag MIR, Moscow, 1981).
[26] A. H. Mueller and B. Patel, Nucl. Phys. **B425**, 471 (1994); A. H. Mueller and G. P. Salam, Nucl. Phys. **B475**, 293 (1996); G. P. Salam, Nucl. Phys. **B461**, 512 (1996);

E. Iancu and A. H. Mueller, Nucl. Phys. **A730**, 460 (2004); **A730**, 494 (2004).
[27] E. Gotsman, E. Levin, and U. Maor, Phys. Rev. D **84**, 051502 (2011).
[28] E. Gotsman, E. Levin, and U. Maor, arXiv:1307.4925.
[29] E. Levin, J. Miller, B. Z. Kopeliovich, and I. Schmidt, J. High Energy Phys. 02 (2009) 048.
[30] B. Z. Kopeliovich, Phys. Rev. C **68**, 044906 (2003); B. Z. Kopeliovich, I. K. Potashnikova, and I. Schmidt, Phys. Rev. C **73**, 034901 (2006).
[31] V. R. Zoller, Z. Phys. C **44**, 207 (1989).
[32] K. G. Boreskov, A. B. Kaidalov, V. A. Khoze, A. D. Martin, and M. G. Ryskin, Eur. Phys. J. C **44**, 523 (2005).
[33] M. M. Block, Phys. Rev. D **84**, 091501 (2011), and references therein.
[34] C. W. De Jagier, H. De Vries, and C. De Vries, At. Data Nucl. Data Tables **14**, 479 (1974).
[35] C. Ciofi degli Atti, B. Z. Kopeliovich, C. B. Mezzetti, I. K. Potashnikova, and I. Schmidt, Phys. Rev. C **84**, 025205 (2011), and references therein.
[36] C. Amsler *et al.* (Particle Data Group), Phys. Lett. B **667**, 1 (2008).
[37] K. Belov, Nucl. Phys. B, Proc. Suppl. **151**, 197 (2006).
[38] S. Knurenko *et al.*, in Proceedings of the 26th International Cosmic Ray Conference, Salt Lake City, 1999, Vol. 1, p. 372 (unpublished).
[39] M. Honda, M. Nagano, S. Tonwar, K. Kasahara, T. Hara, N. Hayashida, Y. Matsubara, M. Teshima, and S. Yoshida (AGASA), Phys. Rev. Lett. **70**, 525 (1993).
[40] M. Aglietta *et al.* (EAS-TOP Collaboration), Phys. Rev. D **79**, 032004 (2009).
[41] G. Aielli *et al.* (ARGO Collaboration), Phys. Rev. D **80**, 092004 (2009).